Amorphous Structures Hot Paper

Deutsche Ausgabe: DOI: 10.1002/ange.201903922
Internationale Ausgabe: DOI: 10.1002/anie.201903922

From Crystalline to Amorphous Germania Bilayer Films at the Atomic Scale: Preparation and Characterization

Adrián L. Lewandowski, Sergio Tosoni, Leonard Gura, Philomena Schlexer, Patrik Marschalik, Wolf-Dieter Schneider, Markus Heyde, Gianfranco Pacchioni, and Hans-Joachim Freund*

Abstract: *A new two-dimensional (2D) germanium dioxide film has been prepared. The film consists of interconnected germania tetrahedral units forming a bilayer structure, weakly coupled to the supporting Pt(111) metal-substrate. Density functional theory calculations predict a stable structure of 558-membered rings for germania films, while for silica films 6-membered rings are preferred. By varying the preparation conditions the degree of order in the germania films is tuned. Crystalline, intermediate ordered and purely amorphous film structures are resolved by analysing scanning tunnelling microscopy images.*

The elucidation of the microscopic structure of amorphous materials is still a subject of intense research. In recent years, the direct observation of a vitreous two-dimensional (2D) silica bilayer (BL) network at the atomic level[1] convincingly confirmed early predictions for the 2D network structure of amorphous oxide surface layers.[2] A concomitant development of appropriate synthesis of ultrathin oxide films and its material characterization applying surface science techniques, specifically scanning probe microscopy comprised the basis of this achievement.

Interestingly, the silica BL can be grown in an amorphous or crystalline variant, depending on the preparation conditions. It has been also observed that the underlying metal substrate promotes one phase or the other.[3] While the crystalline phase consists of a network of 6-membered-rings (MRs), the amorphous one exhibits a distribution of rings of different sizes.[1b,a,3a]

Up to now, the research focus has been on silica model systems, in spite of the significant differences in the atomic arrangements that exist between different glass-former oxide materials.[4]

In this context, amorphous germania is considered a structure-analogue to amorphous silica, that is, a network of corner-sharing XO_4 (X = Si or Ge) tetrahedra.[4b,5] However, germania and silica differ in the degree of distortion of XO_4 unit blocks, and also present a different medium-range order that may be responsible for their considerably different glass transition temperatures.[6,4b] Moreover, germanosilicates are materials with attractive technological and catalytic applications.[7]

In previous studies, we prepared ultrathin films of germania on Ru(0001). A highly ordered monolayer and a buckled amorphous BL were obtained. Their respective microscopic structure was directed by a strong interaction between film and substrate.[8] In the present work, we investigate the growth of ultrathin germania films on a Pt(111) single crystal surface. This metal substrate has been chosen, because it has a similar lattice constant compared to Ru but a lower oxygen affinity.[9] The latter should lead to a weaker film—substrate interaction favoring the structural stability of a BL germania film. BL films of germania have been prepared and studied by scanning tunneling microscopy (STM) as well as density functional theory (DFT) calculations. This new 2D GeO_2 film opens up new opportunities to compare its material properties at the atomic scale, its crystalline-vitreous phase transition conditions to silica. Both materials would be important reference materials for the potential synthesis of silica-germania mixtures.

Recently, A. Malashevich et al. calculated the stability of free-standing germania BL structures.[10] The calculated polymorphs are characterized by a more distorted structure than the analog silica BL structures. They also found that the hexagonal phase, which is formed exclusively by 6 MRs (hexagonal), appear to be 31 meV/Ge more stable than the structure whose unit cell contains one 8 MR and two 5 MRs (558). Our DFT calculations reproduce accurately those results. However, when we introduce Pt(111) as the metal-substrate for the same germania BL structures, the situation changes. The 558 BL, Figure 1 and Table 1, becomes 35 meV/Ge more stable than the hexagonal one.

Both structures consist of two layers of GeO_4 tetrahedra that are connected to each other in the direction perpendicular to the plane of the substrate by sharing an oxygen atom. The angle of the vertical Ge–O–Ge bond, 180° in the hexagonal film, is between 130° and 165° in the 558 one. The distortion of the O–Ge–O bond is one reason why the

[*] A. L. Lewandowski, L. Gura, Dr. P. Marschalik, Prof. W.-D. Schneider, Dr. M. Heyde, Prof. H.-J. Freund
Department of Chemical Physics
Fritz-Haber-Institut der Max-Planck-Gesellschaft
Faradayweg 4–6, 14195 Berlin (Germany)
E-mail: heyde@fhi-berlin.mpg.de
Homepage: http://www.fhi-berlin.mpg.de/cp/
Dr. S. Tosoni, Dr. P. Schlexer, Prof. G. Pacchioni
Department of Materials Science
Università di Milano-Bicocca
Via R. Cozzi, 55, Milan (Italy)
Supporting information and the ORCID identification number(s) for the author(s) of this article can be found under: https://doi.org/10.1002/anie.201903922.

© 2019 The Authors. Published by Wiley-VCH Verlag GmbH & Co. KGaA. This is an open access article under the terms of the Creative Commons Attribution-NonCommercial License, which permits use, distribution and reproduction in any medium, provided the original work is properly cited and is not used for commercial purposes.

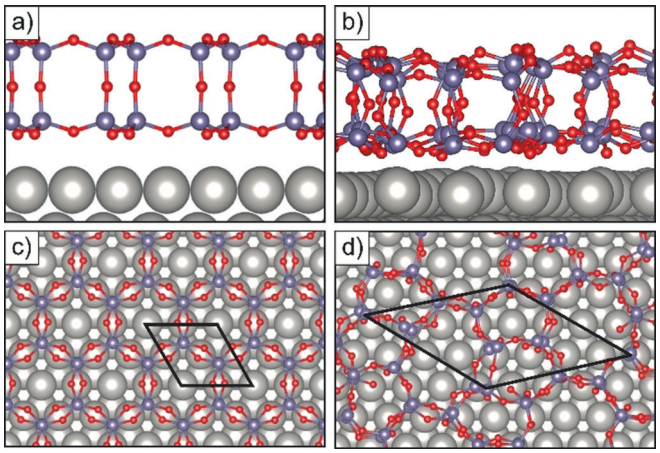

Figure 1. DFT models of the hexagonal and 558 germania bilayer on Pt(111). a) and c) correspond to the side and top view of the hexagonal network, respectively. b) and d) correspond to the side and top view of the 558 structure, respectively. The unit cell is shown in black.

Table 1: Germania bilayer on Pt(111). Adopted Pt(111) supercell, strain (%), interfacial distance (R,Å), adhesion energy (E_{ad},eV nm^{-2}), Bader charge transferred to the germania film (Q, |e| nm^{-2}) and the change in the Pt work function.

	Pt supercell	Strain [%]	R [Å]	E_{ad} [eV nm^{-2}]	Q [|e| nm^{-2}]	$\Delta\phi$ [eV]
Hexagonal	(2×2)	+1.63	2.88	−2.20	−0.34	−0.25
558	$\sqrt{67}\times\sqrt{147}$ R 12°	+0.12 −1.23	2.58	−2.71	−0.66	+0.32

unsupported 558 structure is less favorable than the hexagonal one, but this is compensated by the stronger interaction with the support. Nevertheless, the coupling between the germania BL and the Pt(111) support is much weaker than the previously reported germania BL film on Ru(0001).[8b]

The structure consisting of 6 MRs displays a hexagonal lattice ($a=b=5.47$ Å, $\gamma=120°$). A simple arrangement on the Pt(111) substrate can be obtained if a 1×1 cell of the germania film is superimposed on a 2×2 supercell of Pt(111), whose lattice is also hexagonal. A moderate tensile strain (1.63 %) is released on the germania film. Several registries have been explored by positioning the center of the germania hexagon on a Pt top, bridge and hollow site. The top position was the energetically preferred registry, but the other registries are close in energy (within 0.1 eV). The optimized center-top registry is the one shown in Figure 1 a and c.

The free-standing 558 germania BL has an oblique lattice ($a=11.37$ Å, $b=11.38$ Å, $\gamma=138.9°$). If a large rotated Pt supercell is adopted ($\sqrt{67}\times\sqrt{147}$ R 12°) a good match with a 2×3 GeO_2 supercell is achieved (see Supporting Information), minimizing the strain on the film (+0.12 % and −1.23 % with respect to the two lattice directions), Figure 1 b and d. Given the non-epitaxial character of the interface, and the small influence of the registry on the interaction of the hexagonal structure with the support, other alternative registries have not been explored.

The 558 structure is more strongly bound to the substrate than the hexagonal one (−2.71 and −2.20 eV nm^{-2}, respectively, Table 1). This is the result of the interaction of a metastable, distorted structure with the metal surface: the "promoted" 558 structure binds more strongly, in full analogy with molecular adsorbates.[11] The bonding is dominated by dispersion and the charge transfer from the substrate to the film is small for both structures. The interfacial distance (measured as the average difference in height between the Pt atoms of the topmost layer and bottom oxygen atoms) is larger for the hexagonal (2.88 Å) than for the 558 (2.58 Å), consistent with the stronger bond. The change on the Pt work function is small, but of opposite sign, Table 1. This is the result of three, often cancelling contributions: charge transfer at the interface, intrinsic dipole of the film, and compressive effect.[12]

The difference between the models calculated for silica and germania BLs is caused by the more distorted GeO_4 tetrahedron as compared with the SiO_4 unit block. These findings are consistent with the wider range of the O–Ge–O intratetrahedral angle as compared to O–Si–O that are measured for amorphous bulk silica and germania.[6,13] Those values have been experimentally determined for bulk silica and germania.

We now compare the calculated models with the structures observed experimentally in a coverage range up to two monolayers. At low coverages, a well-defined crystalline monolayer is found (see Supporting Information). With increasing coverage, under similar preparation conditions, BL germania films grow (see Experimental Section). By varying the final annealing temperature three different phases of germania BL films supported on Pt(111) are obtained and analysed. These phases are characterized by a different degree of order, visualized by high-resolution STM images that allow us to study structural features at the atomic scale. The structural analysis involves ring-size distribution, fast Fourier transform (FFT) representation, triplet ring combinations and direct distance orientations (DDOs)[16] of the ring-center positions. The computational methods used for the image analysis are described in the Supporting Information.

Figure 2, left column, shows STM topographic images of three different phases of the germania BL film. The right-hand column in Figure 2 displays in addition color-coded rings which are superimposed onto the images shown in Figure 2, left column. A closer look to the left column in Figure 2 reveals that the three phases exhibit a different degree of order. A mainly crystalline phase is shown in Figure 2 a, a purely amorphous phase in Figure 2 c, while Figure 2 b exhibits an intermediate phase between (a) and (c). Consequently, we refer to the phases of Figure 2 (a), (b), and (c) as the crystalline, the intermediate and the amorphous phase, respectively.

The crystalline germania film is aligned with a high symmetry direction of Pt(111), as determined from the STM images; this differs from the DFT model where the germania BL is rotated by 12° with respect to the substrate in order to reduce the strain from 8–9 % to about 1 %.

 © 2019 Die Autoren. Veröffentlicht von Wiley-VCH Verlag GmbH & Co. KGaA, Weinheim

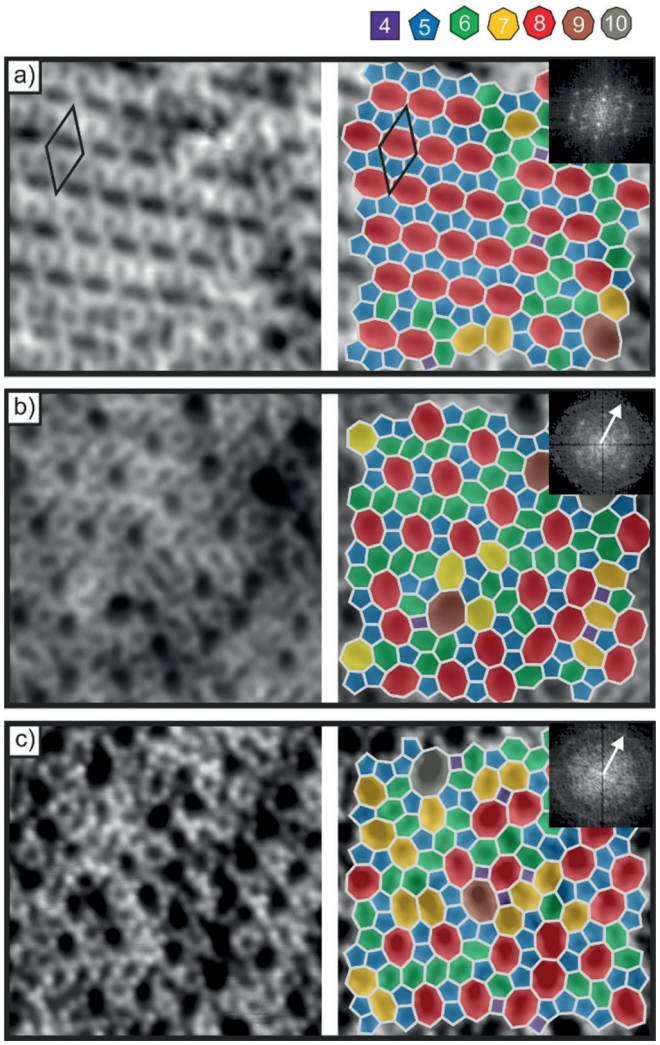

Figure 2. STM images of three phases of the germania bilayer film. The left-hand column shows topographic STM images of scanning size 6.6 nm × 6.6 nm^2. In the right-hand column color-coded rings superimposed on the STM images are added. The ring-sizes are color-coded according to the reference shown at the top right of the Figure. The FFT representation of each STM image is depicted in the top right corner of the right-hand column. a) The unit cell of the crystalline phase is drawn in black. $V_S = 300$ mV, $I_T = 400$ pA. b) $V_S = 600$ mV, $I_T = 200$ pA. c) $V_S = 200$ mV, $I_T = 100$ pA. Size of the FFT: 9.1 × 9.1 nm^{-2}.

The STM image of Figure 2a allows us to distinguish the different ring-sizes forming the film. Interestingly, the main phase shown in Figure 2a exhibits the crystalline structure predicted to be the most stable one for the germania BL on Pt(111), that is, an oblique unit cell (indicated in the Figure) formed by 8 and 5 MRs, as shown above in Figure 1d. The size of the unit cell measured via STM corresponds well to the calculated one. In Figure 2a, one sees a predominantly ordered 558 phase interrupted by straight lines of 6 MRs that introduce anti-phase domain boundaries. Local defects are also recognized through their 7 MRs structures.

In the intermediate phase, depicted in Figure 2b, a dominant phase is no longer visible, although some oriented ring-arrangements without large periodicity are present. The 8 MR orientation follows certain directions and typically join 5 MRs at their sides, while the 6 MRs usually prefer to form straight lines. The periodicity of the mentioned arrangements is interrupted after a few nanometers by a change in direction or by a different ring combination. Therefore, it is difficult to find a repetitive pattern in the medium range order. This phase shows an intermediate behavior between the one of Figure 2a and the phase of Figure 2c that we describe in the next paragraph.

Unlike the signs of order that we observed above in Figure 2a and to a certain extent in Figure 2b, it is difficult to find repeated patterns in the phase shown in Figure 2c, although, on the right side of this image a few chains of the mentioned 558 ring-arrangement are still present.

Apart from that, the distribution and orientation of rings do not follow any preferential orientation. This fact is clearly revealed in the FFT images shown in the insets of Figure 2. In addition, the atomically resolved images allow us to judge the short range order. The corresponding FFT images are shown in the top right corner of the three ring-size structures depicted in the right hand column of Figure 2. The FFT image of the amorphous phase forms a diffuse circle whose radius corresponds to $1/k = 2.6$ Å (indicated with a white arrow in Figure 2c). This distance matches the measured average distance between protrusions that we correlate with the O–O distance of the top-most layer of the film. The measured O–O distance on bulk amorphous germania by XRD is 2.8 Å.[13a] This larger value can be rationalized based on the fact that the oxygen top-most layer in the BL film is not in-plane, a circumstance that is not considered by FFT, nor by measuring distances in real space in STM images. The circle then evidences the random-oriented arrangement of the GeO_4 tetrahedra. The concept of rotationally invariant building blocks is part of the continuous random network model that governs the structure of oxide glasses.[2] The theory was recently corroborated on a 2D vitreous silica.[1a] When looking at the FFT image of the intermediate phase (Figure 2b) the intensity of the circle decreases and some spots emerge. Even more intense spots develop in the FFT representation of Figure 2a. These spots are related to preferential orientations that certain ring-combinations adopt. In particular, the most intense spots of the crystalline phase correspond to the aligned chains of 8 and 5 MRs that predominate in Figure 2a.

The analysis of the ring-size distribution and the preferred ring-combinations for the three different phases presented in Figure 2, yields the ring-size histograms depicted on the left-hand side of Figure 3. At a first glance, there seem to be no major differences between the three ring-size distributions and one can identify a general trend: a clear maximum in the 5 MRs, a few of the largest rings (9 and 10 MRs) and some of the 4 MRs. More than 92% of the rings range from sizes of 5 to 8 MRs. When looking at the histogram of the crystalline phase (Figure 3a) one can see a second maxima distributed between the 6 and the 8 MRs, while the number of 7 MRs is considerably smaller. This ring-size distribution is different from the one of vitreous silica BL on Ru(0001), which consists of an asymmetric distribution around a clear maximum at 6 MRs.[1a,3a] In order to put the information in perspective it is

 © 2019 Die Autoren. Veröffentlicht von Wiley-VCH Verlag GmbH & Co. KGaA, Weinheim

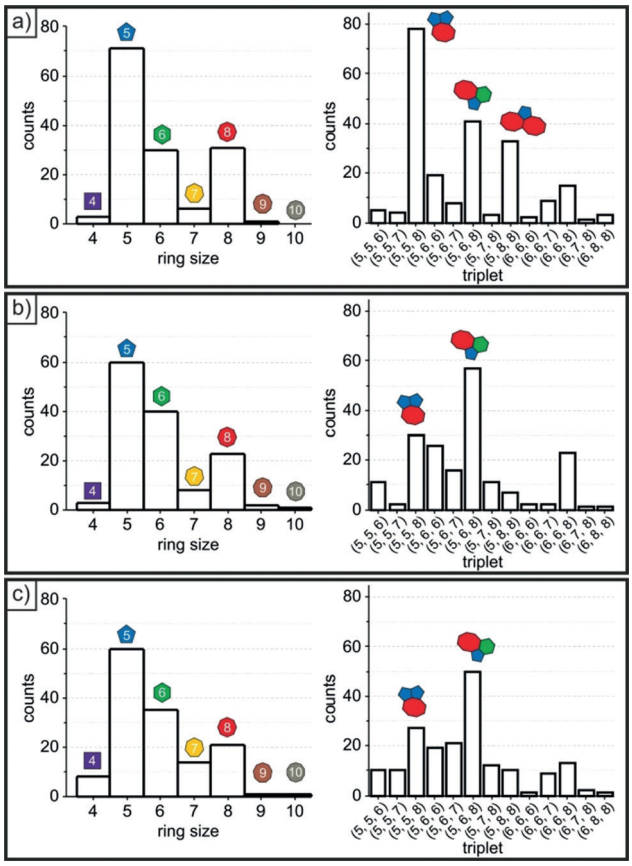

Figure 3. Ring-size histogram and triplet combination analysis of three phases of the germania bilayer film. The analysis shown in Figure a), b), and c) correspond to the phases depicted in Figure 2a, b, and c, respectively. Ring-size histograms of the three phases are shown in the left-hand side of the Figure. The right-hand side exhibits triplet combination analsis for each phase. For clarity, only the most prominent triplet combinations are shown.

important to consider the metal substrate, as we have recently realized when analyzing silica BL films supported on a Pt(111) single-crystal. The ring-size distribution is different from the one reported for silica BL on Ru(0001) (see Supporting Information).

With decreasing crystallinity the ring-size distribution, indicated in Figure 3a to Figure 3c, changes. The amount of 8 and 5 MRs decreases progressively, while the number of 7 MRs increases and the number of 6 MRs stays more or less constant. In order to get a deeper quantitative insight into these subtle phase changes reflected in the histograms, we investigate the connectivity of the ring structure as a function of the crystalline order of the system.

We analyzed the occurring triplet combinations in which three rings share the same connection point (vertex). For the given images the total numbers of occurring triplet combinations are 19, 25, and 31 for the crystalline, the intermediate and the amorphous phase, respectively (see Supporting Information).

The most prominent triplet combinations are plotted in the right-hand column of Figure 3. On the horizontal axis the ring sizes participating to each triplet are listed in brackets. As expected, the (5,5,8) is the most frequent triplet in the crystalline phase, followed by the (5,6,8) triplet present in the boundary structures. In the intermediate and amorphous phases, the (5,6,8) triplet combination is more abundant and the amount of (5,5,8) loses predominance, although it is still a preferred combination. The (6,6,6) triplet combination is very rare for all the germania BL phases.

In contrast, amorphous silica BL presents a small number of the (5,5,8) triplet combination while the (6,6,6) predominates.[14] These observations are in line with the DFT results showing a lack of 6 MRs as discussed above. Moreover, the most prevalent antiphase boundary in the crystalline silica BL is formed by a linear arrangement of (5,5,8) ring-combinations.[15]

A DDO analysis[16] provides further insight into the observed phase change from crystalline to amorphous germania. The left-hand column in Figure 4 shows again the ring-network from Figure 2, right column. Now, black straight lines connect the center of adjacent rings to each other. The angle which these connecting lines form with respect to the

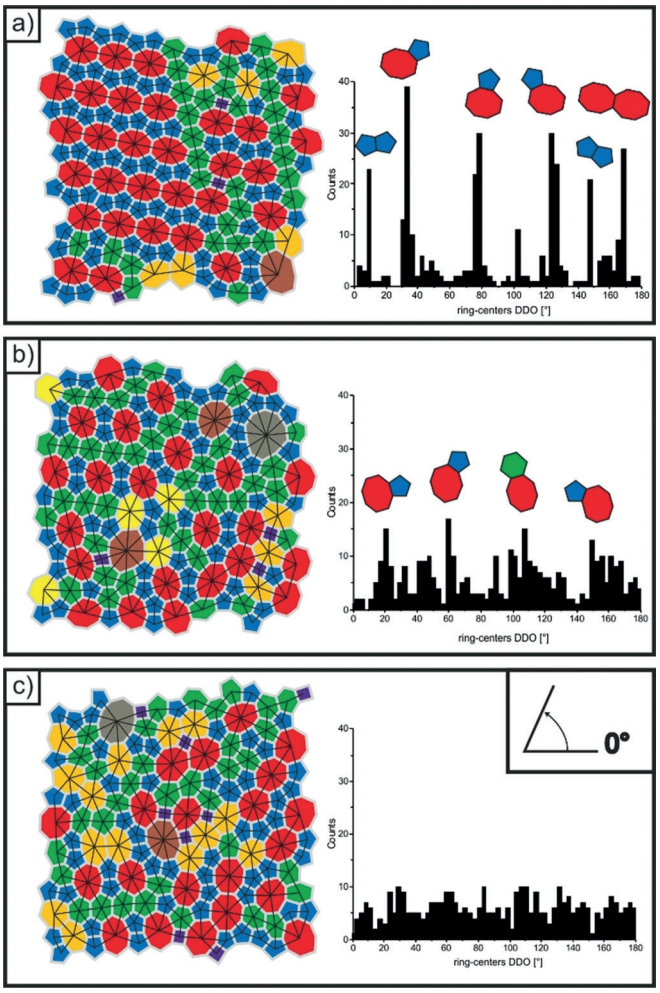

Figure 4. DDO analysis of the ring-center positions. On the left-hand side the network derived from Figure 2 is shown. The ring-center positions of adjacent rings are connected with black lines. The angle formed between two neighboring rings is measured with respect to the 0° shown at the top right corner of Figure 4c. The most frequent pair-combinations are drawn next to the corresponding peaks.

 © 2019 Die Autoren. Veröffentlicht von Wiley-VCH Verlag GmbH & Co. KGaA, Weinheim

reference of zero degree, (shown in a box in the top right corner of Figure 4c), is plotted for each phase in the right-hand column of Figure 4. While the crystalline phase exhibits several well-defined peaks (Figure 4a), the amorphous phase shows non-preferential ring-ring orientations (Figure 4c). These results confirm the discussed FFT representations. The germania film shown in Figure 4b exhibits an intermediate behavior: small peaks evidence the preferred orientation of a few ring pairs.

The DDO analysis allows us to correlate the most prominent peaks with the involved ring sizes. In Figure 4, right column, next to each peak, the contributing most relevant ring pairs are indicated. Interestingly, in almost all cases the 8 MRs are responsible for the presence of pair of rings following specific orientations. In particular, the pair-combination of the 5 MRs connecting preferentially to six of the eight available sides of the elongated 8 MRs corresponds to the most frequent oriented couple for the crystalline and intermediate phase (Figure 4a and b). The orientations of the elongated 8 MRs in the crystalline phase are 120° rotated with respect to the 8 MRs in the intermediate phase (see Figure 4a and b). We have observed also the presence of domains, which are rotated 120° with respect to each other, in different areas of the crystalline film (see large-scale STM image of the crystalline film provided in the Supporting Information). The influence of the hexagonal Pt(111) substrate may be responsible for the 3-fold orientation of the film.

In conclusion, a new 2D germanium dioxide model-system was successfully synthesized and characterized. By varying the preparation conditions we created crystalline and vitreous structures, which we imaged and characterized in real space. One significant difference between the germania film discussed here and the earlier prepared and characterized silica film is the glass transition temperature which is known for the bulk materials, that is, 1480 K for silica[17] and 980 K for germania.[18] For the films that is also manifested in the annealing temperatures used to prepare amorphous silica (1170–1270 K) and germania (800–900 K) BLs. Our studies open up experimental avenues to study the dynamics of those transitions at the atomic scale. Importantly, for the germania BL structure on Pt(111) we have found experimentally a unit cell consisting of a 558 ring-combination as the most stable one, thus confirming the DFT preferable structure. In perspective, with the present study a general understanding of the structure of oxide network forming glasses comes a little closer.

Experimental Section

All experiments are carried out in ultra-high vacuum (UHV) conditions (base pressure 10^{-10} mbar range). The imaging is done at room temperature with a beetle-type STM using a PtIr tip. The preparation of germania BL films on Pt(111) is based on that of germania films on Ru(0001)[8] (see Supporting Information).

The three different phases presented here correspond to films prepared at different final annealing temperatures that range from 800 to 900 K. The higher the temperature, the more ordered the film is.

Periodic DFT calculations were performed using the Vienna Ab Initio Simulation Package (VASP),[19,20] the Perdew, Burke, and Ernzerhof (PBE) functional[21] and the projector augmented wave (PAW) method.[22,23] Dispersion forces were included with the D2′ approach.[24,25]

Acknowledgements

This project has received funding from the European Research Council (ERC) under the European Union's Horizon 2020 Research and Innovation Program (Grant Agreement No. 669179).

Conflict of interest

The authors declare no conflict of interest.

Keywords: amorphous structures · crystalline materials · germania · scanning probe techniques · thin films

How to cite: *Angew. Chem. Int. Ed.* **2019**, *58*, 10903–10908
Angew. Chem. **2019**, *131*, 11019–11024

[1] a) L. Lichtenstein, C. Büchner, B. Yang, S. Shaikhutdinov, M. Heyde, M. Sierka, R. Wlodaczyk, J. Sauer, H.-J. Freund, *Angew. Chem. Int. Ed.* **2012**, *51*, 404–407; *Angew. Chem.* **2012**, *124*, 416–420; b) D. Löffler, J. J. Uhlrich, M. Baron, B. Yang, X. Yu, L. Lichtenstein, L. Heinke, C. Büchner, M. Heyde, S. Shaikhutdinov, H.-J. Freund, R. Włodarczyk, M. Sierka, J. Sauer, *Phys. Rev. Lett.* **2010**, *105*, 146104.

[2] W. H. Zachariasen, *J. Am. Chem. Soc.* **1932**, *54*, 3841–3851.

[3] a) P. Y. Huang, S. Kurasch, A. Srivastava, V. Skakalova, J. Kotakoski, A. V. Krasheninnikov, R. Hovden, Q. Mao, J. C. Meyer, J. Smet, D. A. Muller, U. Kaiser, *Nano Lett.* **2012**, *12*, 1081–1086; b) X. Yu, B. Yang, J. A. Boscoboinik, S. Shaikhutdinov, H.-J. Freund, *Appl. Phys. Lett.* **2012**, *100*, 151608; c) H. Tissot, X. Weng, P. Schlexer, G. Pacchioni, S. Shaikhutdinov, H.-J. Freund, *Surf. Sci.* **2018**, *678*, 118; d) E. I. Altman, J. Götzen, N. Samudrala, U. D. Schwarz, *J. Phys. Chem. C* **2013**, *117*, 26144–26155.

[4] a) P. S. Salmon, A. C. Barnes, R. A. Martin, G. J. Cuello, *J. Phys. Condens. Matter* **2007**, *19*, 415110; b) M. Micoulaut, L. Cormier, G. S. Henderson, *J. Phys. Condens. Matter* **2006**, *18*, 753.

[5] a) B. E. Warren, *J. Am. Ceram. Soc.* **1934**, *17*, 249–254; b) B. E. Warren, *Phys. Rev.* **1934**, *45*, 657.

[6] J. D. E. Desa, A. C. Wright, R. N. Sinclair, *J. Non-Cryst. Solids* **1988**, *99*, 276–288.

[7] a) C. Duverger, S. Turrell, M. Bouazaoui, M. F. Tonelli, M. Montagne, M. Ferrari, *Philos. Mag. B* **1998**, *77*, 363–372; b) T. Blasco, A. Corma, M. J. Díaz-Cabañas, F. Rey, J. A. Vidal-Moya, C. M. Zicovich-Wilson, *J. Phys. Chem. B* **2002**, *106*, 2634–2642.

[8] a) A. L. Lewandowski, P. Schlexer, C. Büchner, E. M. Davis, H. Burrall, K. M. Burson, W.-D. Schneider, M. Heyde, G. Pacchioni, H.-J. Freund, *Phys. Rev. B* **2018**, *97*, 115406; b) A. L. Lewandowski, P. Schlexer, S. Tosoni, L. Gura, P. Marschalik, C. Büchner, H. Burall, K. M. Burson, W.-D. Schneider, G. Pacchioni, M. Heyde, *J. Phys. Chem. C* **2019**, *123*, 7889–7897.

[9] C. N. R. Rao, P. Vishnu Kamath, S. Yashonath, *Chem. Phys. Lett.* **1982**, *88*, 13.

[10] A. Malashevich, S. Ismail-Beigi, E. I. Altman, *J. Phys. Chem. C* **2016**, *120*, 26770–26781.

[11] C. Morin, D. Simon, P. Sautet, *J. Phys. Chem. B* **2004**, *108*, 5653–5665.

[12] S. Prada, U. Martinez, G. Pacchioni, *Phys. Rev. B* **2008**, *78*, 235423.

 © 2019 Die Autoren. Veröffentlicht von Wiley-VCH Verlag GmbH & Co. KGaA, Weinheim

[13] a) D. L. Price, M.-L. Saboungi, A. C. Barnes, *Phys. Rev. Lett.* **1998**, *81*, 3207; b) A. C. Wright, *J. Non-Cryst. Solids* **1994**, *179*, 84 – 115.
[14] C. Büchner, L. Liu, S. Stuckenholz, K. M. Burson, L. Lichtenstein, M. Heyde, H.-J. Gao, H.-J. Freund, *J. Non-Cryst. Solids* **2016**, *435*, 40 – 47.
[15] K. M. Burson, C. Büchner, M. Heyde, H.-J. Freund, *J. Phys. Condens. Matter* **2017**, *29*, 035002.
[16] a) L. Lichtenstein, M. Heyde, H.-J. Freund, *J. Phys. Chem. C* **2012**, *116*, 20426 – 20432.
[17] P. Richet, Y. Bottinga, L. Denielou, J. P. Petitet, C. Tequi, *Geochim. Cosmochim. Acta* **1982**, *46*, 2639 – 2658.
[18] P. Richet, *Phys. Chem. Miner.* **1990**, *17*, 79 – 88.
[19] G. Kresse, J. Hafner, *Phys. Rev. B* **1993**, *47*, 558 – 561.
[20] G. Kresse, J. Furthmüller, *Comput. Mater. Sci.* **1996**, *6*, 15 – 50.
[21] J. P. Perdew, K. Burke, M. Ernzerhof, *Phys. Rev. Lett.* **1996**, *77*, 3865 – 3868.
[22] P. E. Blöchl, *Phys. Rev. B* **1994**, *50*, 17953 – 17979.
[23] G. Kresse, D. Joubert, *Phys. Rev. B* **1999**, *59*, 1758 – 1775.
[24] S. Grimme, *J. Comput. Chem.* **2006**, *27*, 1787 – 1799.
[25] S. Tosoni, J. Sauer, *Phys. Chem. Chem. Phys.* **2010**, *12*, 14330 – 14340.

Manuscript received: March 31, 2019
Accepted manuscript online: May 3, 2019
Version of record online: July 1, 2019

 © 2019 Die Autoren. Veröffentlicht von Wiley-VCH Verlag GmbH & Co. KGaA, Weinheim